Hindawi Publishing Corporation
Advances in Tribology
Volume 2011, Article ID 837469, 8 pages
doi:10.1155/2011/837469

Research Article

Wear Behavior and Its Correlation with Mechanical Properties of TiB_2 Reinforced Aluminium-Based Composites

N. B. Dhokey and K. K. Rane

Department of Metallurgy and Material Science, Government College of Engineering, Pune 411005, India

Correspondence should be addressed to N. B. Dhokey, nbdhokey@yahoo.co.in

Received 3 July 2011; Revised 1 August 2011; Accepted 22 August 2011

Academic Editor: Luca Settineri

Aluminium-based TiB_2 reinforced composite is a promising material to be used as brake drum material, and it may emerge as substitute for conventional gray cast iron. Aluminium-based composites containing 2% by wt copper reinforced with 2.5 and 5 wt% TiB_2 composites were made in induction furnace by in situ synthesis process using simultaneous addition of halide fluxes (K_2TiF_6 and KBF_4). These cast composites were evaluated for microstructures, hardness, flow curve properties, and tensile properties. It was observed that overall wear behavior gave reasonably good correlation with mechanical properties of composites as compared to gray cast iron.

1. Introduction

Metal matrix composite containing ceramic particulates tends to improve mechanical properties as well as wear properties by way of creating restriction to deformation of material during mechanical working. Metal matrix composites (especially aluminium and titanium based) are used in aerospace and automobile industries due to their enhanced properties such as modulus, hardness, tensile strength, and wear resistance combined with significant weight saving [1, 2]. Aluminium with ceramic reinforcements such as Al_2O_3, SiC, TiC, and TiB_2 are used for structural applications, for their good toughness and wear resistance [3]. Modulus of composite increases with TiC- and TiB_2-particle additions and it is greater than that for composite with Al_2O_3 and SiC. Also, interfacial bonding is enhanced in the TiC- and TiB_2-added composites [4]. There are different techniques of forming TiB_2 in the matrix such as powder metallurgy method, spray, deposition and several casting methods such as rheocasting, squeeze casting, stir-casting and compo casting [5, 6]. Different systems are used for synthesis of this composite such as TiO_2-Al-B, TiO_2-Al-B-CuO, TiO_2-Al-B_2O_3, $NaBH_4$, and $TiCl_4$ and Ti-containing and B-containing salts are added to the melt resulting in a series of chemical reactions which produce submicron TiB_2 particles within the melt [3, 7, 8]. The addition of reinforcement produces increase in strength and stiffness over the base alloy at the expense of ductility as compared to cast aluminium [4, 9]. The wear rate of the composites improves significantly with the TiB_2 content. The friction coefficient also decreased with increasing TiB_2 content, which indicates decrease in wear rate and hence the improvement in the wear resistance of the composite [10, 11]. Wear and mechanical properties of commercially used grades of cast irons (GI250, GIHC, GI 250Ti, and CGI) suggest that compact graphite cast iron exhibits higher mechanical strength among all grades, but it has less wear resistance than other grades of cast irons [12].

It is well known that application of Al-MMC in automotive components can reduce the weight of the vehicle by one third over gray cast iron. The aim of the present work is to establish a correlation of wear behavior with mechanical properties of the Al-TiB_2 composites as compared to gray cast iron.

2. Materials and Experimental Methods

2.1. Materials and Processing. Commercially pure (CP) aluminium was taken as matrix material. In situ flux assessed

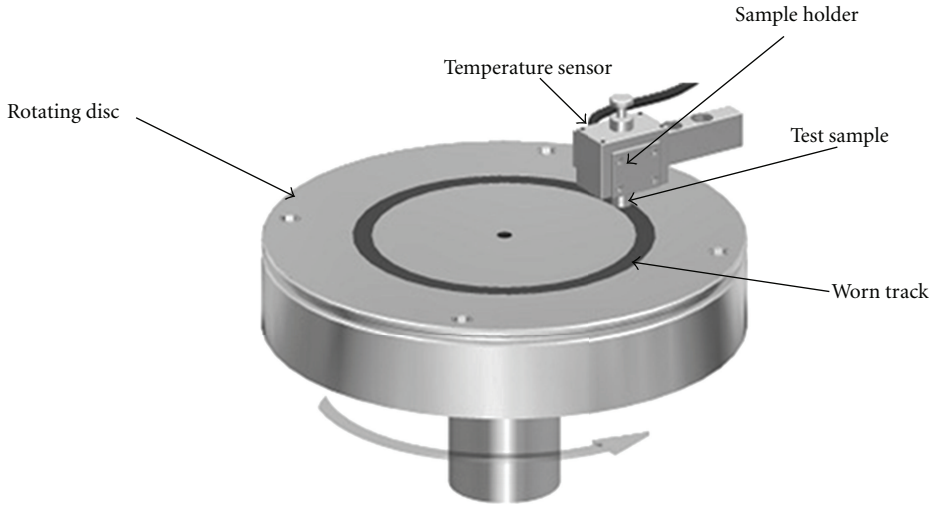

Figure 1: Schematic configuration of Pin-on-Disc machine employed for wear test.

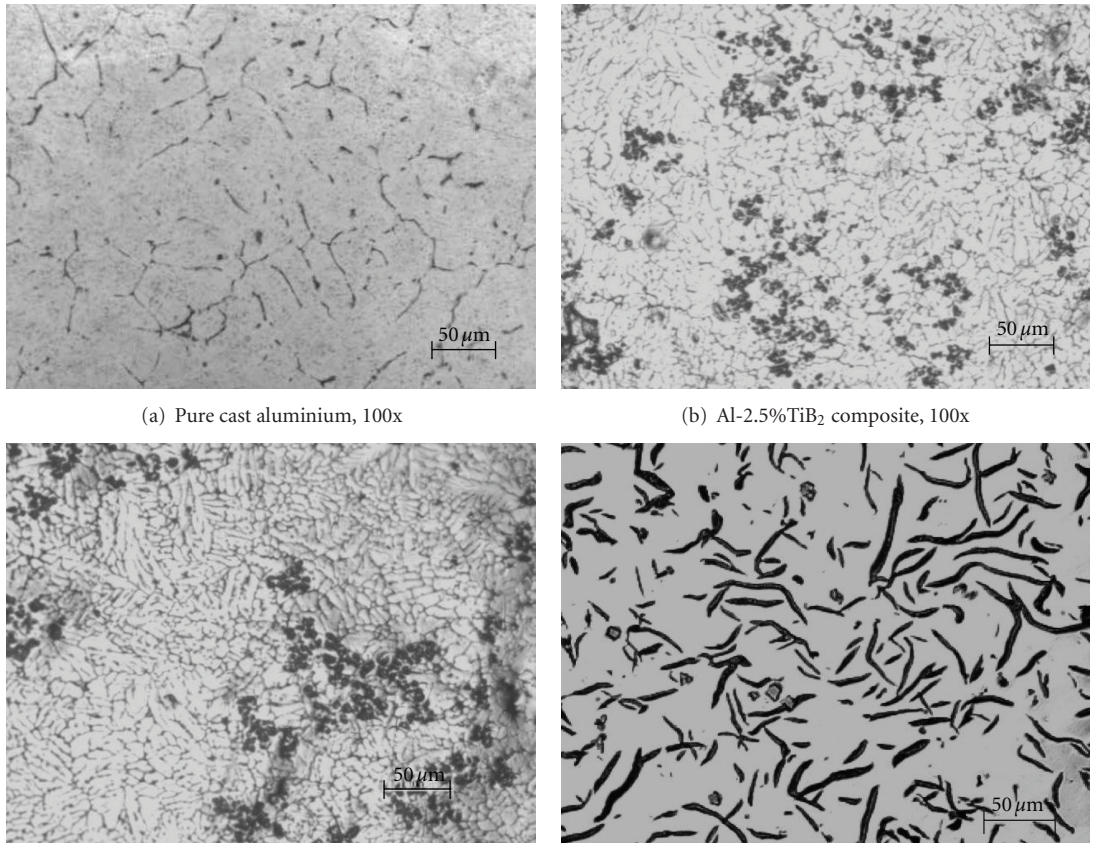

(a) Pure cast aluminium, 100x

(b) Al-2.5%TiB_2 composite, 100x

(c) Al-5%TiB_2 composite, 100x

(d) Gray cast iron, 100x

Figure 2: Optical micrographs of cast aluminium, Al-2.5%TiB_2 Al-5%TiB_2 composite and gray cast iron.

synthesis technique was used to form TiB_2-reinforced composite by using commercially available fluoride based fluxes that is, potassium hexafluorotitanate (K_2TiF_6) and potassium tetrafluororate (KBF_4). In situ synthesis process was adopted for the fabrication of the composite. Individual fluxes that is, potassium hexafluorotitanate (K_2TiF_6) and potassium tetrafluororate (KBF_4), were added together in molten aluminium and reacted as given by (1)

$$K_2TiF_6 + 2KBF_4 + \left(\frac{22}{3}\right)Al \longrightarrow TiAl_3 + AlB_2 + 3KAlF_4 + \left(\frac{1}{3}\right)K_3AlF_6 \quad (1)$$

$$AlB_2 + TiAl_3 \longrightarrow TiB_2 + 4Al$$

Formation of TiB_2 is greatly influenced by the presence of AlB_2 and Al_3Ti in molten aluminium. But due to the fact that

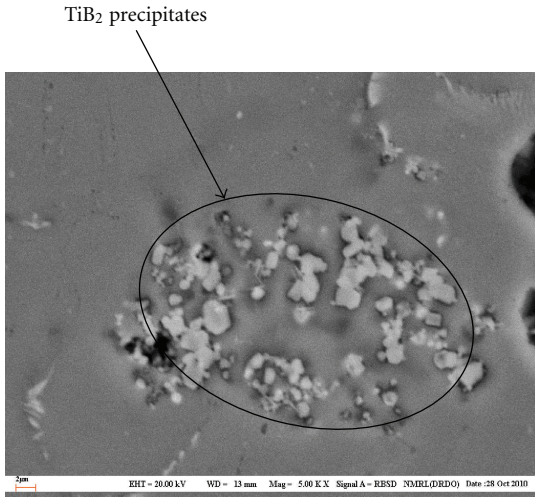

Figure 3: SEM micrograph shows magnified image of segregated pockets of TiB_2 in aluminium matrix at 5000x.

Gibbs free energy for formation of Al_3Ti is higher than AlB_2, the recovery of boron is lower [13]. Hence 20% extra KBF_4 addition compared to stoichiometric amount was made to reduce the presence of allied products and complete the reaction to produce TiB_2 reinforcement [14]. The properties of synthesized composites were compared with gray cast iron used for brake drum of automotive applications and it consists of 3.54% C, 2.15% Si and 0.51% Mn (by wt).

Induction furnace (25 KW, Make Autocontrol, Mumbai) was used for making the composites with controlled argon shrouding and as well as for gray cast iron as the reference material. After sufficient holding time and degasing of melt, the molten composite was poured into preheated mould (200°C) to get cast specimens of dimensions 150 mm length and 20 mm diameter for material charaterisation.

2.2. Material Characterization. Reinforcement phases were observed in scanning electron microscope (make-JOEL, Japan). Samples for SEM analysis were polished by using electrolytic polishing machine (Eletropol Metatech) with a flow of electrolyte solution (Methanol-730 mL, Butyl Cellosolve-98 mL, Perchloric acid-78 mL and Distilled water-100 mL). Additionally, for revealing grain boundaries of matrix and reinforcement distribution, the etching was carried out using Villella reagent (20 mL Hydrofluoric acid, 10 mL Nitric acid, 30 mL Glycerin).

The hardness of composite was measured by using micro hardness machine (FM-700, Future-tech). The load applied was 100 gram with dwell time of 15 seconds. An average of six readings was reported.

Tensile test specimens were made as per ASTM A 370 standard and tested in a Universal Testing Machine (Capacity 10 Tons). The average data values of three samples obtained from tensile test were used. In the same machine, compression testing was carried on specimen having $L/D = 1$ ($D = 20$ mm). The specimen was gradually pressed in compression in steps of 1000 Kg, and its instantaneous height and diameter were recorded to get true stress verses true strain plot, using an average of three test specimens. The corresponding flow curve equation was derived for each composite studied

$$\sigma = k \times \epsilon^n, \tag{2}$$

where σ = true stress in MPa, ϵ = true strain, and n = strain hardening exponent.

Pin-on-Disc wear test machine (M/s Magnum Engineers, Bangalore) was used for wear analysis. Pin specimen (Ø 10 mm) was kept stationary perpendicular to disc, while the circular disc (SAE 52100 steel, 61 HRC, 0.3 μRA, and disc diameter 165 mm) was rotated as shown in Figure 1. A load of 60 N and sliding velocity 1.8 m/s was employed for wear rate evaluation. An average wear rate was reported based on three samples of same composition. In order to find out the rise in temperature during wear test, temperature sensor was positioned in 1 mm diameter drilled hole at 15 mm distance from sliding end of the specimen.

3. Results and Discussion

3.1. Microstructural Analysis. Optical microstructure of Al-TiB_2 composites with different reinforcement content are shown in Figure 2. As compared to pure aluminium, average grain size of phase in composite is relatively small.

3.2. SEM Microstructure. Figure 3 shows microstructure of Al-5% TiB_2 composite segregated spot of TiB_2 (Figure 3) in the aluminium matrix. Typically, TiB_2 particles are present in the segregated manner due to high interfacial energy.

3.3. SEM-EDS Analysis with Elemental Distribution. SEM-EDS analysis was used to ascertain approximate chemical composition of reinforcement and also that of matrix. Figure 4 indicate spectrum of Al-5% TiB_2 composite with peaks of aluminium and titanium. EDS elemental analysis indicated in Figure 5 confirms the presence of TiB_2 precipitates. Figure 6 shows elemental distribution that confirms the presence of boron, aluminium, and titanium.

3.4. Microhardness Analysis. The hardness of composite with different reinforcement content was compared with gray cast iron as reference material. Figure 7 shows variation of Al-MMC for varying reinforcement content of TiB_2. Al-based composite containing 2.5 wt% TiB_2 indicate 47% improvement in hardness and this goes up with increasing TiB_2 content. It is noticed that hardness of 5% TiB_2 is increased by almost twice than that of pure aluminium but much less than that of gray cast iron.

3.5. Mechanical Properties

3.5.1. Tensile Properties. It is evident from Table 1 that the composite exhibited higher UTS and higher fracture strength than aluminium with reduced ductility. The significant improvement in the mechanical properties of the composite

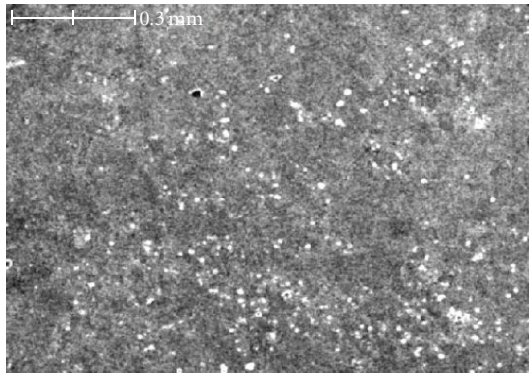

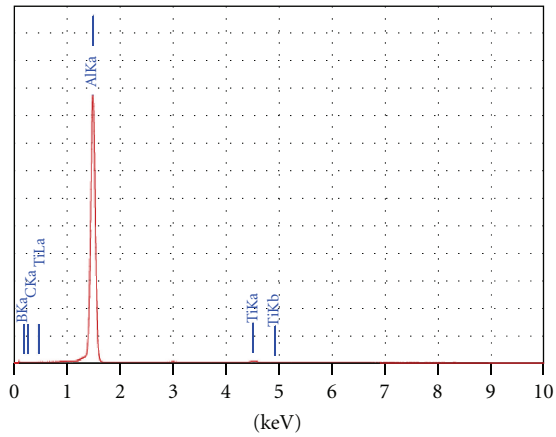

Element	(keV)	Mass (%)	At (%)
B	—	—	—
Al	1.486	97.67	98.67
Ti	4.508	2.33	1.33
Total		100	100

Figure 4: EDX spectrum and elemental mapping of Al-5%TiB_2 composite.

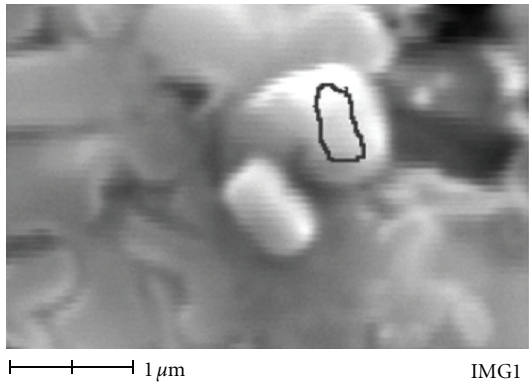

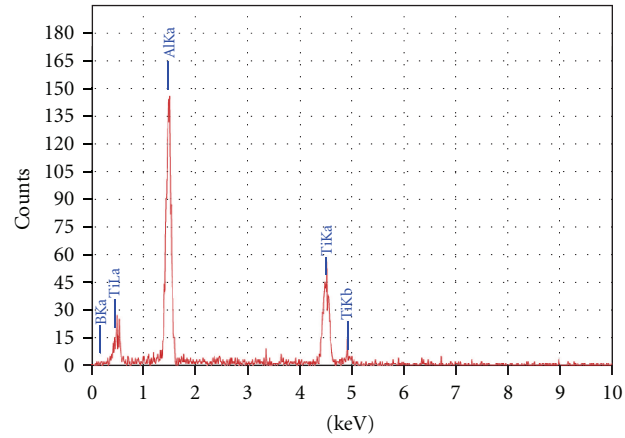

Element	(keV)	Mass (%)	At (%)
B	0.183	42.45	70.26
Al	1.486	28.47	18.88
Ti	4.508	29.08	10.86
Total		100	100

Figure 5: EDX spectrum and elemental mapping on TiB_2 particle.

Table 1: Data of tensile test conducted on cast Al, Al-MMCs and gray cast iron.

Sr. no.	Properties	Pure aluminium	Al-2.5%TiB_2	Al-5%TiB_2	Gray cast iron
1	Y.S (MPa)	74	93	96	—
2	UTS (MPa)	121	157	180	284
3	Fracture strength (MPa)	70	78	150	284
5	%Reduction in area	22.53	16.84	9.38	3.19
6	%Elongation	8	6.5	6	3

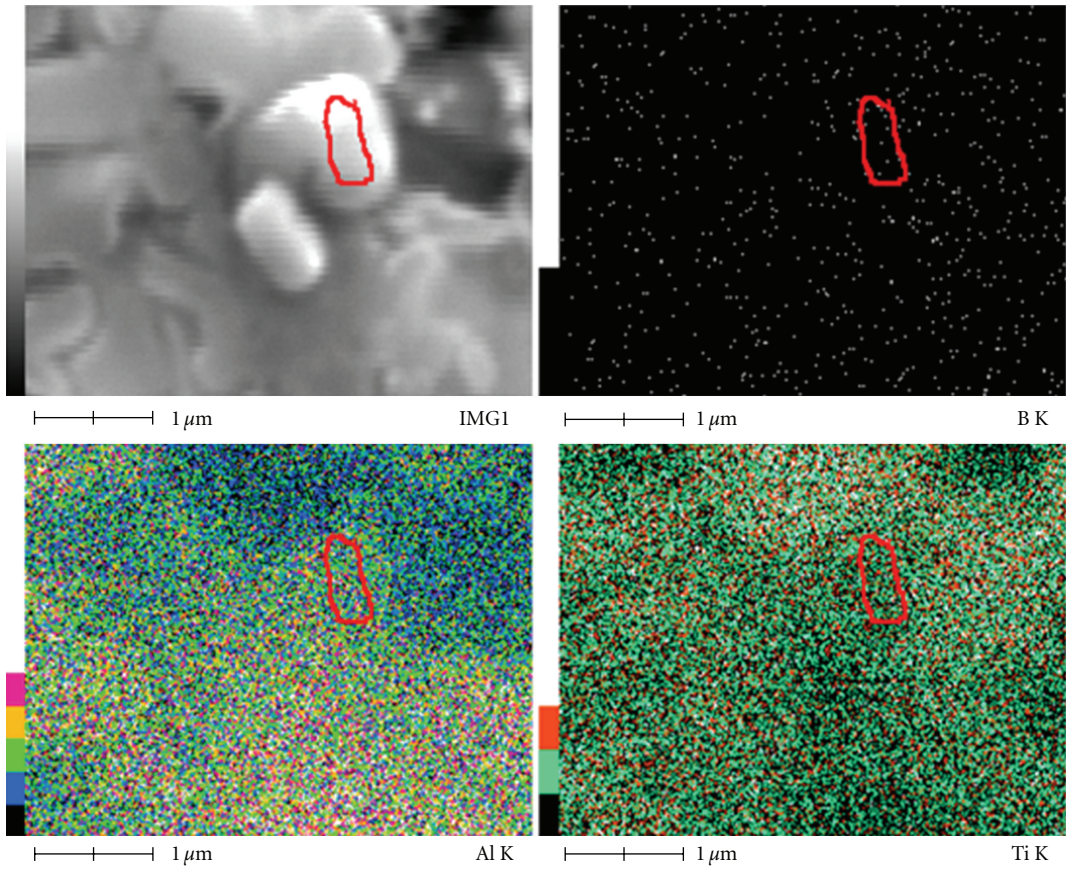

Figure 6: Elemental distribution of boron, aluminium, titanium nearby TiB_2 clusters.

Table 2: Flow curve properties of composite materials.

Sr. no.	Properties	Pure aluminium	Al-2.5%TiB_2	Al-5%TiB_2
1	K (MPa)	137	138	141
2	n	0.412	0.375	0.324
3	Gross increase in area (along radial direction)	56.25%	45.56%	42.12%
4	Gross reduction in height (along longitudinal direction)	34.5%	31.5%	28.5%

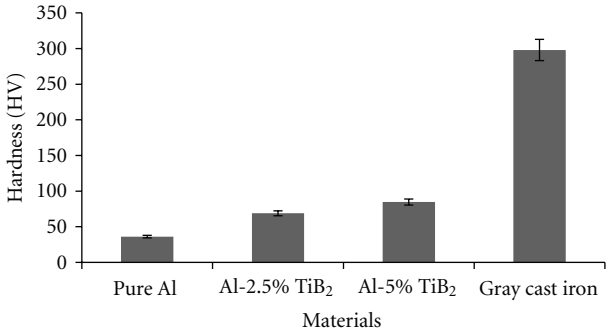

Figure 7: Hardness variation of cast aluminium, Al-TiB_2 composites, and gray cast iron.

as compared with the aluminium can be attributed to TiB_2 particles in the matrix. Similar trend of increasing tensile properties is reported by previous researchers in case of Al-12% by wt. TiB_2 and Al-4.5% Cu-3% C-15%TiB_2 composites [15, 16]. The fractured surfaces as depicted in Figure 8 shows a shift in fracture behavior from ductile to brittle; for example, pure aluminium indicates cup and cone type ductile fracture, Al-5% TiB_2 reveals mixed mode ductile-brittle transition, and gray cast iron shows brittle fracture.

3.5.2. Flow Curve Properties. Compression test results are plotted in the form of flow curve, and the corresponding properties derived from flow curve equation are given in Table 2. It can be observed that strength coefficient (K) increases with increase in reinforcements, whereas strain hardening decreases with increased TiB_2 content. Overall, higher TiB_2 content shows higher strain hardening rate (n). It means that composite exhibits appreciable deformation behavior which can be seen from gross deformation both in transverse as well as in longitudinal direction.

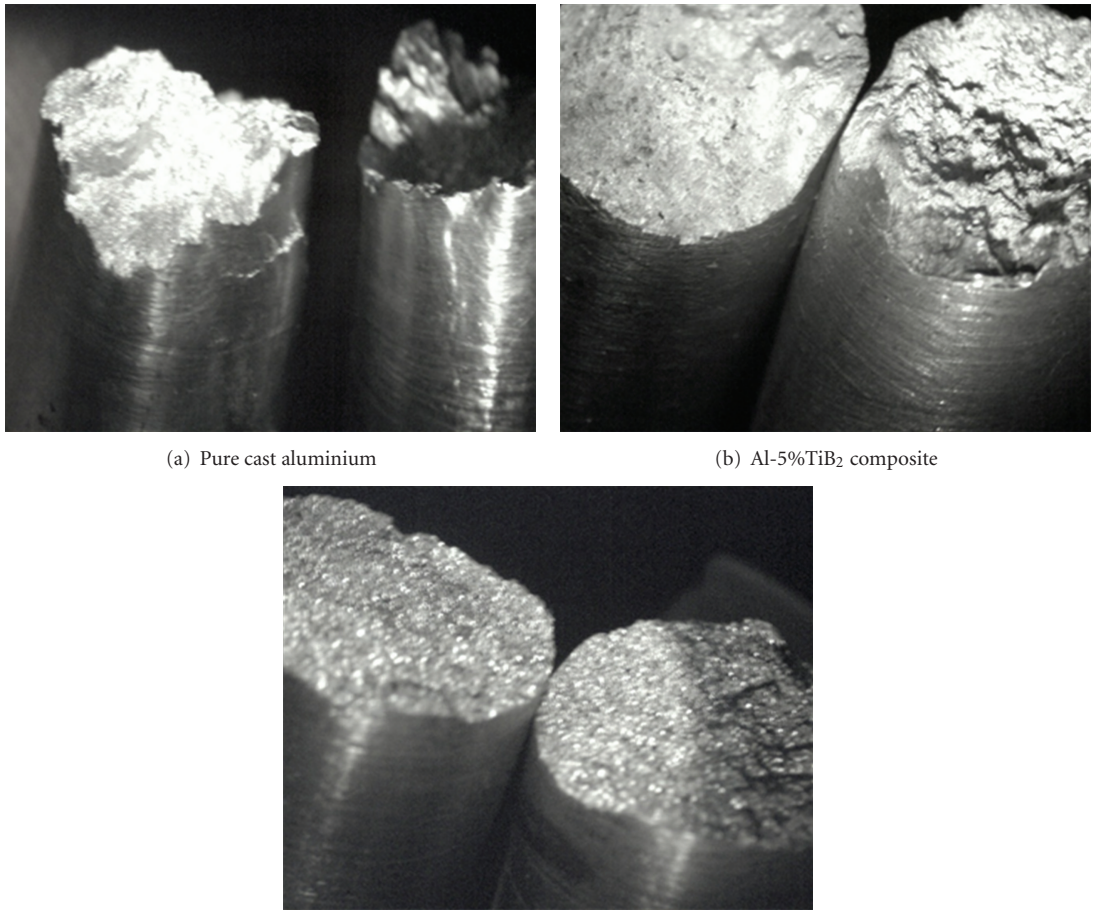

(a) Pure cast aluminium

(b) Al-5%TiB_2 composite

(c) Gray cast iron, 100x

Figure 8: Stereomicrographs of tensile fractured surfaces of (a) Cast aluminium, (b) Al-5%TiB_2 composite and (c) Gray cast iron.

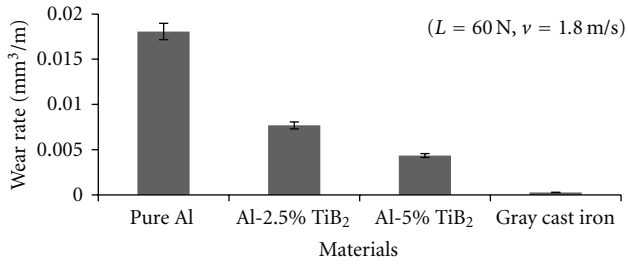

Figure 9: Wear rate variation of sliding pins made out of different materials.

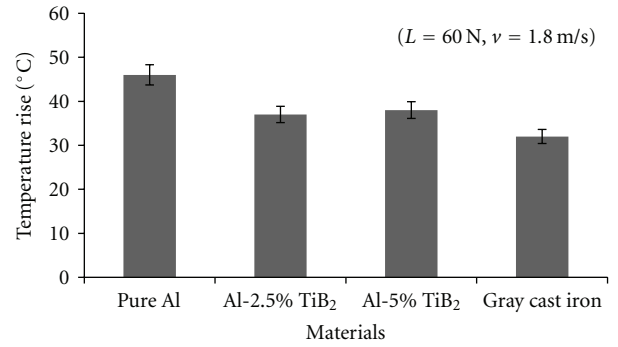

Figure 10: Temperature rise variation of sliding pins made out of different materials.

3.6. Sliding Wear Analysis. Figure 9 shows the variation of wear rate with composition for MMCs. Apparently, pure aluminium exhibits the highest wear loss whereas gray cast iron shows the lowest wear loss, for the given set of applied load and sliding speed employed. Al-based composite shows a decrease in wear rate with increasing content of TiB_2 reinforcement which acts as obstacle to shear deformation, while material is getting slid on the counterface. However, wear rate is much higher than gray cast iron. Also, TiB_2 acts as load-bearing element in the matrix. This supports the work reported elsewhere in TiB_2-reinforced Al-7%Si alloy [17]. Figure 10 shows that temperature rise during sliding is more for pure aluminium and its composites than that of gray cast iron. It is well known that aluminum exhibits high thermal conductivity (237 W/m·K), and it reduces with increasing addition of TiB, while gray cast iron has relatively low thermal conductivity (70 W/m·K). It can be noted that

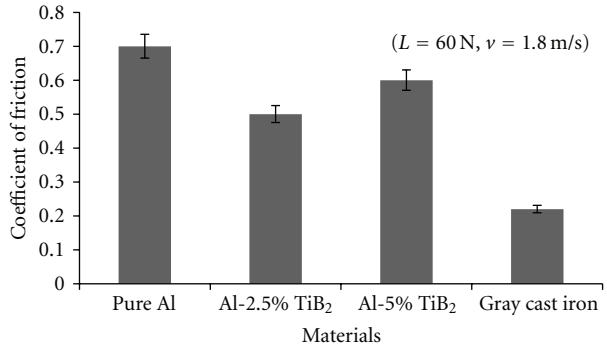

Figure 11: Coefficient of friction variation of sliding pins made out of different materials.

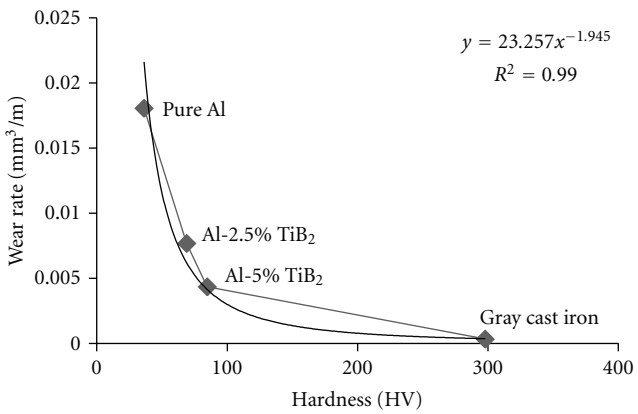

Figure 12: Effect of hardness on wear rates of composites.

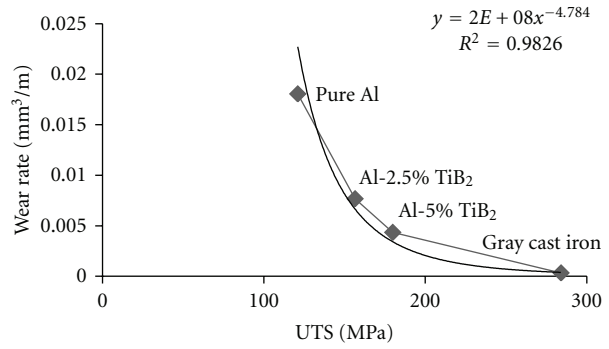

Figure 13: Effect of ultimate tensile strength on wear rate of composites.

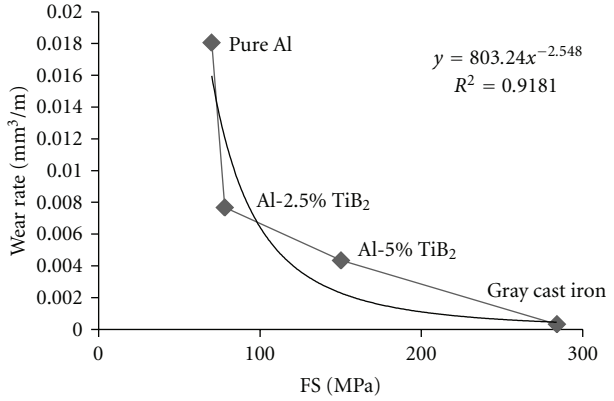

Figure 14: Effect of fracture strength on wear rates of composites.

the addition of TiB_2 particle to the aluminium matrix gives some effect on reducing the coefficient of friction as evident in Figure 11. The variation in the average coefficient of friction for the pure aluminium and composites varies in the range of 0.5–0.7 which is much larger than that of gray cast iron (0.21).

4. Correlation of Mechanical Properties with Wear Behavior

Wear is a complex phenomenon and governed not only by hardness, but also by other influencing parameters like microstructure, method of processing, thermal properties of the sliding material, and mechanical properties [18]. A correlative wear model based on mechanical, thermal, physical properties and process parameters has been attempted to understand wear complexity [19].

Various plots of mechanical properties as derived from tensile test and compressive test are plotted to establish correlation with wear properties. It is noted that wear rate shows approximate power law relationship with hardness (Figure 12), UTS (Figure 13), fracture stress (Figure 14), strength coefficient (Figure 15), and strain hardening exponent (Figure 16). All these relationship, give R^2 value that is much higher than 0.9, indicting strong effect of mechanical properties on wear rates. It may be noted that mechanical properties are strongly affected by reinforcement in microstructures. Thus, volumetric wear rate follows certain trend with hardness of the material validating Archard's equation [20]. Similar effort of finding out correlation of Young's modulus and hardness on wear resistance was made for alloys with different elemental addition of La, Mg, Pd, and Zr. It was found out that hardness and Young's modulus both correlate well with wear resistance for Al-Ni group of alloys [21].

5. Conclusions

Based on the forgoing discussion of Al-MMCs and its relative comparison with gray cast iron, the following conclusions can be drawn.

(1) Mechanical properties are strongly affected by the content of TiB_2 in Al-MMCs.

(2) Wear behavior gives a reasonable correlation with hardness, ultimate tensile strength, fracture strength, and strain hardening exponent of Al-MMCs. The relationship between wear rate and mechanical properties validates Archard's equation.

(3) Wear rate decreases with increasing TiB_2 content.

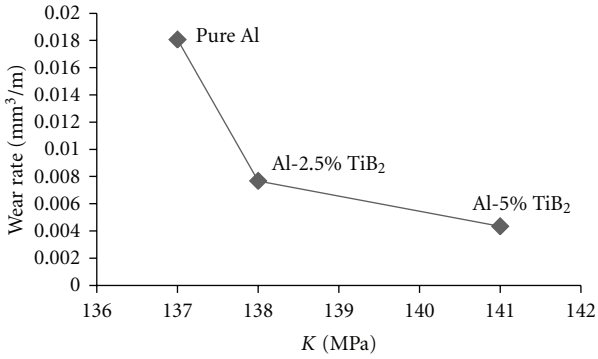

Figure 15: Effect of strengthening coefficient on wear rate of composites.

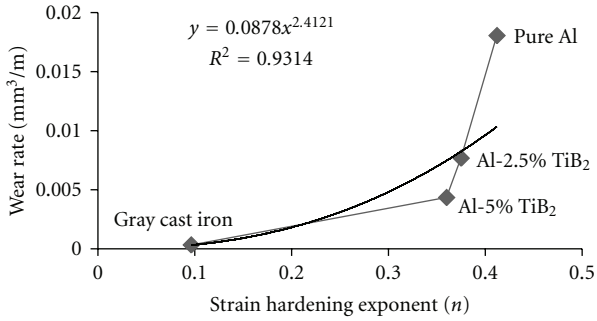

Figure 16: Effect of strain hardening exponent on wear rate of composites.

Acknowledgments

The authors thank the University Grant Commission, India for providing financial support for this research. Thanks and appreciations are also extended to the Director, College of Engineering, Pune, and VNIT Nagpur for providing SEM facility.

References

[1] T. Zeuner, P. Stojanov, P. R. Sahm, H. Ruppert, and A. Engels, "Developing trends in disc brake technology for rail application," *Materials Science and Technology*, vol. 14, no. 9-10, pp. 857–863, 1998.

[2] R. Dwivedi, "Development of advanced reinforced aluminum brake rotors," *SAE Technical Paper Series*, vol. 104, no. 5, pp. 159–166, 1995.

[3] S. C. Tjong, S. Q. Wu, and H. G. Zhu, "Wear behavior of in situ $TiB_2 \cdot Al_2O_3$/Al and $TiB_2 \cdot Al_2O_3$/Al-Cu composites," *Composites Science and Technology*, vol. 59, no. 9, pp. 1341–1347, 1999.

[4] A. R. Kennedy, A. E. Karantzalis, and S. M. Wyatt, "The microstructure and mechanical properties of TiC and TiB_2-reinforced cast metal matrix composites," *Journal of Materials Science*, vol. 34, no. 5, pp. 933–940, 1999.

[5] Y. Han, X. Liu, and X. Bian, "In situ TiB2 particulate reinforced near eutectic Al-Si alloy composites," *Composites—Part A*, vol. 33, no. 3, pp. 439–444, 2002.

[6] M. J. Koczak and M. K. Premkumar, "Emerging technologies for the in-situ production of MMCs," *JOM*, vol. 45, no. 1, pp. 44–48, 1993.

[7] L. Shi, Y. Gu, L. Chen, Z. Yang, J. Ma, and Y. Qian, "A convenient solid-state reaction route to nanocrystalline TiB_2," *Composites*, vol. 36, no. 2, pp. 1177–1187, 2005.

[8] F. C. Wang, Z. H. Zhang, J. Luo, C. C. Huang, and S. K. Lee, "A novel rapid route for in situ synthesizing TiB-TiB_2 composites," *Composites Science and Technology*, vol. 69, no. 15-16, pp. 2682–2687, 2009.

[9] D. G. Zhao, X. F. Liu, Y. C. Pan, X. F. Bian, and X. J. Liu, "Microstructure and mechanical properties of in situ synthesized (TiB_2 + Al_2O_3)/Al-Cu composites," *Journal of Materials Processing Technology*, vol. 189, no. 1–3, pp. 237–241, 2007.

[10] A. Mandal, B. S. Murty, and M. Chakraborty, "Sliding wear behaviour of T6 treated A356-TiB_2 in-situ composites," *Wear*, vol. 266, no. 7-8, pp. 865–872, 2009.

[11] S. Natarajan, R. Narayanasamy, S. P. Kumaresh Babu, G. Dinesh, B. Anil Kumar, and K. Sivaprasad, "Sliding wear behaviour of Al 6063/TiB_2 in situ composites at elevated temperatures," *Materials and Design*, vol. 30, no. 7, pp. 2521–2531, 2009.

[12] G. Cueva, A. Sinatora, W. L. Guesser, and A. P. Tschiptschin, "Wear resistance of cast irons used in brake disc rotors," *Wear*, vol. 255, no. 7–12, pp. 1256–1260, 2003.

[13] L. Lü, M. O. Lai, Y. Su, H. L. Teo, and C. F. Feng, "In situ TiB_2 reinforced Al alloy composites," *Scripta Materialia*, vol. 45, no. 9, pp. 1017–1023, 2001.

[14] N. B. Dhokey, S. Ghule, K. Rane, and R.S. Ranade, "Effect of KBF_4 and K_2TiF_6 on precipitation kinetics of TiB_2 in aluminium matrix composite," *Journal of Advance Material Letters*, vol. 2, no. 3, pp. 210–216, 2011.

[15] K. L. Tee, L. Lü, and M. O. Lai, "Improvement in mechanical properties of in-situ Al-TiB_2 composite by incorporation of carbon," *Materials Science and Engineering A*, vol. 339, no. 1-2, pp. 227–231, 2003.

[16] T. V. Christy, N. Murugan, and S. Kumar, "A comparative study on the microstructures and mechanical properties of Al 6061 Alloy and the MMC Al 6061/TiB_2," *Journal of Minerals & Materials Characterization & Engineering*, vol. 9, no. 1, pp. 57–65, 2010.

[17] S. Kumar, M. Chakraborty, V. Subramanya Sarma, and B. S. Murty, "Tensile and wear behaviour of in situ Al-7Si/TiB_2 particulate composites," *Wear*, vol. 265, no. 1-2, pp. 134–142, 2008.

[18] S. C. Lim and M. F. Ashby, "Overview no. 55 Wear-Mechanism maps," *Acta Metallurgica*, vol. 35, no. 1, pp. 1–24, 1987.

[19] N. B. Dhokey and R. K. Paretkar, "Study of wear mechanisms in copper-based SiCp (20% by volume) reinforced composite," *Wear*, vol. 265, no. 1-2, pp. 117–133, 2008.

[20] J. F. Archard, "Contact and rubbing of flat surfaces," *Journal of Applied Physics*, vol. 24, no. 8, pp. 981–988, 1953.

[21] A. L. Greer, K. L. Rutherford, and I. M. Hutchings, "Wear resistance of amorphous alloys and related materials," *International Materials Reviews*, vol. 47, no. 2, pp. 87–112, 2002.